J|A|C|S ARTICLES

Published on Web 01/30/2009

High-Lamellar Ordering and Amorphous-Like π-Network in Short-Chain Thiazolothiazole−Thiophene Copolymers Lead to High Mobilities

Itaru Osaka,[†] Rui Zhang,[†] Geneviève Sauvé,[†] Detlef-M. Smilgies,[‡] Tomasz Kowalewski,*[,†] and Richard D. McCullough*[,†]

Department of Chemistry, Carnegie Mellon University, Pittsburgh, Pennsylvania 15213, and Cornell High Energy Synchrotron Source, Cornell University, Ithaca, New York 14853

Received March 17, 2008; E-mail: tomek@andrew.cmu.edu; rm5g@andrew.cmu.edu

Abstract: Owing to their superior transport properties, poly(alkylthiophenes) and their derivatives emerged as one of the most widely studied semiconducting polymers with potential applications in organic electronics. It is now generally acknowledged that one of the particularly effective ways to increase the carrier mobility in these materials is by increasing the length of the conjugated backbones. Some recent reports suggest also that carrier mobilities can be further enhanced by highly crystalline arrangement (and interdigitation) of alkyl side chains possibly because it promotes the formation of extensive layered structures favorable for carrier transport. Results presented here demonstrate that, surprisingly, none of these factors are actually necessary for good electronic performance of polythiophene-like systems. Thiophene-based semiconducting polymers bearing thiazolothiazole unit (PTzQT) described here were shown to have very high carrier mobilities (~0.3 cm^2/Vs) despite their low molecular weight and uneven spacing of alkyl side chains, which suppressed high side chain crystallinity/interdigitation as revealed by thermal analysis and X-ray scattering. The highly disordered nature of these materials extended to the nanoscale level as evident from atomic force microscopy images, which have shown only the presence of small domains packed into isotropic amorphous-like superstructures with lateral correlation lengths increasing with the length of alkyl side chains. The observed concomitant increase of carrier mobilities points to the possible role of characteristic length of surface roughness as the key parameter controlling carrier transport in disordered, noninterdigitating systems.

Introduction

Polymer semiconductors have been attracting much attention since they seem destined to offer low-cost, flexible, and throwaway electronic applications, such as organic field-effect transistors (OFETs), organic thin film solar cells, or radio frequency identification (RFID) tags.[1] This new class of plastic materials is of great advantage in this area since devices can be fabricated by simple printing techniques.[2] Overall progress in this field has been driven, in part, by the development of regioregular polythiophenes where, for example, regioregular poly(3-hexylthiophene) (rrP3HT) has become a standard,[3] which has led to the further development of various kinds of thiophene-based polymer semiconductors.[4−12] One of the key design constraints in rr-polythiophene semiconductors is the regular placement of side chains which promotes a flat backbone and crystalline structures which, in turn, leads to good electronic performance. Some recently introduced new regiosymmetric structures, such as poly(5,5′-bis(3-dodecyl-2-thienyl)-2,2′-

[†] Carnegie Mellon University.
[‡] Cornell University.

(1) (a) *Organic Electronics: Materials, Manufacturing and Applications*; Klauk, H., Ed.; Wiley-VCH: Weinheim, Germany, 2006. (b) *Semiconducting Polymers: Chemistry, Physics and Engineering*; Hadziioannou, G., Malliaras, G. G., Eds.; Wiley-VCH: Weinheim, Germany, 2007. (c) *Handbook of Conducting Polymers: Third Edition*; Skotheim, T. A., Reynolds, J. R., Ed.; CRC Press: Boca Raton, FL, 2007. (d) Sirringhaus, H; Tessler, N.; Friend, R. H. *Science* **1998**, *280*, 1741–1744. (e) Huitena, H. E. A.; Gelinck, G. H.; van der Putter, J. B. P. H.; Kuijk, K. E.; Hart, C. M.; Cantatore, E.; Herwig, P. T.; van Breemen, A. J. J. M.; de Leeuw, D. M. *Nature* **2001**, *414*, 599. (f) Bao, Z. *Adv. Mater.* **2000**, *12*, 227–230. (g) Li, Y. N.; Wu, Y. L.; Ong, B. S. *Macromolecules* **2006**, *39*, 6521. (h) Dimitrakopoulos, C. D.; Malenfant, P. R. L. *Adv. Mater.* **2002**, *14*, 99.

(2) (a) Katz, H.; Bao, Z. *J. Phys. Chem.* **2000**, *B104*, 671–678. (b) Sirringhaus, H.; Brown, P. J.; Friend, R. H.; Nielsen, M. M.; Bechgaard, K.; Langeveld-Voss, B. M. W.; Spiering, A. J. H.; Janssen, R. A. J.; Meijer, E. W.; Herwig, P.; de Leeuw, D. M. *Nature* **1999**, *401*, 685–688. (c) Kline, R. J.; McGehee, M. D.; Toney, M. F. *Nat. Mater.* **2006**, *5*, 222–228. (d) Sirringhaus, H. *Adv. Mater.* **2005**, *17*, 2411–2425. (e) Sirringhaus, H.; Kawase, T.; Friend, R. H.; Shimoda, T.; Inbasekaran, M.; Wu, W.; Woo, E. P. *Science* **2000**, *290*, 2123–2126.

(3) (a) McCullough, R. D.; Lowe, R. D. *J. Chem. Soc., Chem. Commun.* **1992**, 70. (b) McCullough, R. D.; Lowe, R. D.; Jayaraman, M.; Anderson, D. L. *J. Org. Chem.* **1993**, *58*, 904. (c) McCullough, R. D. *Adv. Mater.* **1998**, *10*, 93–116. (d) Chen, T.; Rieke, R. D. *J. Am. Chem. Soc.* **1992**, *114*, 10087.

(4) Sirringhaus, H.; Wilson, R. J.; Friend, R. H.; Inbasekaran, M.; Wu, W.; Woo, E. P.; Grell, M.; Bradley, D. D. C. *Appl. Phys. Lett.* **2000**, *77*, 406.

(5) (a) Ong, B. S.; Wu, Y.; Liu, P.; Gardner, S. *J. Am. Chem. Soc.* **2004**, *126*, 3378. (b) Wu, Y.; Liu, P.; Gardner, S.; Ong, B. S. *Chem. Mater.* **2005**, *17*, 221.

(6) (a) Li, Y.; Wu, Y.; Liu, P.; Birau, M.; Pan, H.; Ong, B. S. *Adv. Mater.* **2006**, *18*, 3029. (b) Pan, H.; Li, Y.; Wu, Y.; Liu, P.; Ong, B. S.; Zhu, S.; Xu, S. *Chem. Mater.* **2006**, *18*, 3237. (c) Pan, H.; Li, Y.; Wu, Y.; Liu, P.; Ong, B. S.; Zhu, S.; Xu, G. *J. Am. Chem. Soc.* **2007**, *129*, 4112.

10.1021/ja801475h CCC: $40.75

Scheme 1. Synthetic Route and Chemical Structure of Poly(2,5-bis(3-alkyl-5-(3-alkylthiophen-2-yl)thiophen-2-yl)thiazolo[5,4-*d*]thiazole)s (PTzQTs)

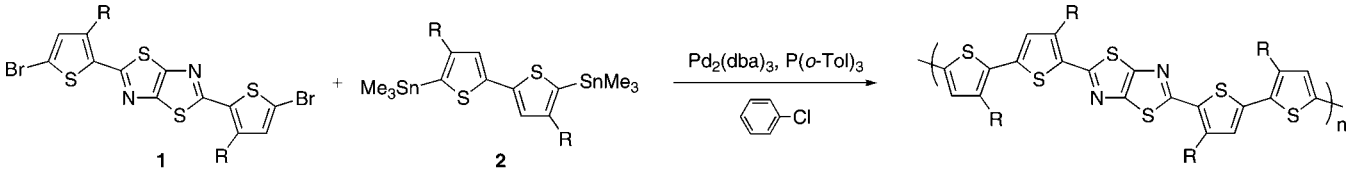

PTzQT-6 (R=C_6H_{13})
PTzQT-12 (R=$C_{12}H_{25}$)
PTzQT-14 (R=$C_{14}H_{29}$)

bithiophene) (PQT)[5a] and poly(2,5-bis(3-alkylthiophene-2-yl)thieno[3,2-*b*]thiophene)s (PBTTTs),[7b] have been reported to even exceed the high-field-effect mobility of rrP3HT presumably owing to the higher ordered, crystalline packed structures found in thin films.

Of particular interest here are some recent reports by Kline et al. which indicate that the molecular ordering of conjugated polymer backbones is highly sensitive to the molecular packing of polythiophene side chains.[13] In particular, they pointed out that PBTTTs and PQT, both of which have low side chain attachment density and uniform side chain arrangement (and thus promote efficient side chain packing and interdigitation), exhibit a high degree of three-dimensional packing of adjacent polymer backbones, strong π stacking, and a high degree of lamellar order. They then went on to propose that these highly ordered crystalline structures facilitate the high performance of those polymers in the OFET devices. They also pointed out the contrast between these structures and familiar rrP3HT, which, while also forming crystalline π stacks, exhibits no side chain interdigitation/ordering and has only limited lamellar order.

Recently, we have reported on a related thiophene-based copolymer incorporating a rigid fused thiazolothiazole ring in the backbone, poly(2,5-bis(3-dodecyl-5-(3-dodecylthiophen-2-yl)thiophen-2-yl)thiazolo[5,4-*d*]thiazole)s (**PTzQT-12**).[14] Despite its low molecular weight, this interesting polymer showed a high-field-effect mobility of $\sim$0.14 cm^2/Vs with a high current on/off ratio of $\sim 10^6$. The design of the PTzQTs takes into account several design constraints that could lead to high-performance semiconducting polymers. The use of thiazolothiazole-fused ring ensures a very rigid and coplanar backbone and thereby highly extended π-electron system and strong π stacking. The electron-deficient nature of the thiazolothiazole affords high oxidative stability. However, the uneven placement of the alkyl side chains along the backbone can be expected to suppress interdigitation and to promote amorphous-like π-stacking and π-connectivity along the chain while enhancing solubility. In regard to side chain arrangement, the key difference between PTzQTs and PBTTT/PQT is that while the side chains in PTzQTs are still arranged regiosymmetrically, they are not equally spaced along the backbone. As will be shown here, as a consequence, the side chains are apparently disordered and do not interdigitate as seen in PBTTT or PQT. Most interestingly, despite all these factors, X-ray diffraction patterns of PTzQTs indicate very strong lamellar ordering, and field-effect transistors fabricated from these materials show high-field-effect mobilities. All these results appear quite surprising in view of earlier mentioned findings on the role of side chain interdigitation/ordering and indicate that the strong interdigitation and formation of extended regular terracelike structures are not the necessary condition for high carrier mobility in polythiophene-like materials.

In this paper, we report a deeper investigation of electronic, morphological, and physical properties of PTzQTs with different side chains (hexyl, dodecyl, and tetradecyl) offering more detailed morphological and microstructural studies on the polymer thin films that reveal how the short-chain PTzQTs can lead to excellent OFET performance with mobilities as high as 0.3 cm^2/Vs. We also evaluate the effect of side chain length on the surface morphology, the lateral correlation length of nanometer/micrometer domains, the microstructures, and the OFET performances including mobility and stability of solution-cast thin films of PTzQT. The results shown here give a new insight for designing high-performance semiconducting polymers. Presented insights are expected to inspire new molecular designs of high-performance semiconducting polymers which, by virtue of being less dependent on the formation of long-range-ordered structures, could be more suitable for rapid mass fabrication of plastic electronic devices.

Experimental Section

Materials. Monomers **1** and **2** were synthesized according to the previous paper.[14] The synthesis of poly(2,5-bis(3-dodecyl-5-(3-dodecylthiophen-2-yl)thiophen-2-yl)thiazolo[5,4-*d*]thiazole)(**PTzQT-12**) has also been previously reported.[14] ^{1}H NMR spectra were measured in $CDCl_3$ as the deuterated solvent using BRUKER Avance 300 NMR spectrometer.

Poly(2,5-bis(3-hexyl-5-(3-hexylthiophen-2-yl)thiophen-2-yl)-thiazolo[5,4-d]thiazole) (PTzQT-6). A solution of **1** (190 mg, 0.3 mmol), **2** (198 mg, 0.3 mmol), tris(dibenzylideneacetone)dipalladium (0) (5.5 mg, 0.006 mmol), and tri-*o*-tolylphosphine (7.3 mg, 0.024 mmol) in 10 mL of anhydrous chlorobenzene was refluxed for 3 days under N_2 atmosphere. After cooling to 50 °C, the reaction solution was poured into 200 mL of methanol

(7) (a) Heeney, M.; Bailey, C.; Genevicius, K.; Shkunov, M.; Sparrowe, D.; Tierney, S.; McCulloch, I. *J. Am. Chem. Soc.* **2005**, *127*, 1078. (b) McCulloch, I.; Heeney, M.; Bailey, C.; Genevicius, K.; MacDonald, I.; Shkunov, M.; Sparrowe, D.; Tierney, S.; Wagner, R.; Zhang, W.; Chabinyc, M. L.; Kline, R. J.; McGehee, M. D.; Toney, M. F. *Nat. Mater.* **2006**, *5*, 328.
(8) Usta, H.; Lu, G.; Facchetti, A.; Marks, T. J. *J. Am. Chem. Soc.* **2006**, *128*, 9034.
(9) Zhang, M.; Tsao, H. N.; Pisula, W.; Yang, C.; Mishra, A. K.; Müllen, K. *J. Am. Chem. Soc.* **2007**, *129*, 3472.
(10) Zhu, Y.; Champion, R. D.; Jenekhe, S. A. *Macromolecules* **2006**, *39*, 8712.
(11) Liu, J.; Zhang, R.; Sauvé, G.; Kowalewski, T.; McCullough, R. D. *J. Am. Chem. Soc.* **2008**, *130*, 13167.
(12) Fong, H. H.; Pozdin, V. A.; Amassian, A.; Malliaras, G. G.; Smilgies, D.-M.; He, M.; Gasper, S.; Zhang, F.; Sorensen, M. *J. Am. Chem. Soc.* **2008**, *130*, 13202.
(13) Kline, R. J.; DeLongchamp, D. M.; Fischer, D. A.; Lin, E. K.; Richter, L. J.; Chabinyc, M. L.; Toney, M. F.; Heeney, M.; McCulloch, I. *Macromolecules* **2007**, *40*, 7960.
(14) Osaka, I.; Sauvé, G.; Zhang, R.; Kowalewski, T.; McCullough, R. D. *Adv. Mater.* **2007**, *19*, 4160.

containing 5 mL of hydrochloric acid and was stirred for 5 h. Then, the precipitated dark brown solid was subjected to sequential Soxhlet extraction with methanol and hexane to remove low molecular weight fraction of the material. The residue was extracted with chloroform to yield 198 mg of dark brown metallic product after removing chloroform and drying in vacuo (yield = 82%). ^{1}H NMR ($CDCl_3$, δppm): 7.04 (br, 4H), 2.90 (br, 8H), 1.74 (br, 8H), 1.30 (br, 24H), 0.90 (br, 12H).

Poly(2,5-bis(3-tetradecyl-5-(3-tetradecylthiophen-2-yl)thiophen-2-yl)thiazolo[5,4-d]thiazole) (PTzQT-14). The title polymer was synthesized as described for **PTzQT-6** to yield 347 mg of dark brown metallic product (yield = 92%). ^{1}H NMR ($CDCl_3$, δ ppm): 7.04 (br, 4H), 2.90 (br, 8H), 1.74 (br, 8H), 1.30 (br, 88H), 0.90 (br, 12H).

Measurements. Molecular weight of the polymer was evaluated through gel permeation chromatography (GPC) calibrated by polystyrene standard with chloroform as an eluent using Waters 2690 separation module equipped with three 5 μm Phenogel columns connected in series (guard, 10^5, 1000, and 100 Å) and a Waters 2487 dual λ absorbance UV detector. UV−vis absorption spectra were measured using VARIAN Cary 5000 UV−vis−NIR spectrophotometer. The thermal properties were analyzed using Seiko Instruments Inc. DSC 220 with temperature range of 0−350 °C at a rate of 10 °C/min in both heating and cooling processes. Cyclic voltammetric measurement was performed on AUTOLAB PGSTAT100 system with a three-electrode cell of which the working electrode was coated with a polymer thin film from a polymer solution in chloroform in a solution of tetrabutylammonium hexafluorophosphate (^{n}Bu$_4$NPF$_6$) in acetonitrile (0.1 M). Ag/AgCl electrode, platinum wire, and platinum disk were used as reference, counter, and working electrodes, respectively. The values of ionization potential (IP) (E_{HOMO}) were estimated using the equations $E_{HOMO} = E_{OX} + 4.4$, where E_{OX} is the onset potential of oxidation versus SCE.[15] Tapping-mode atomic force microscopy (AFM) study was carried out with the aid of Digital Instruments Nanoscope III-M system equipped with a J-type vertical scanner. The AFM observations were performed at room temperature in air using silicon cantilevers with nominal spring constant of 50 N/m and nominal resonance frequency of 300 Hz (standard silicon TESP probes). A typical value of AFM detector signal, corresponding to an rms cantilever oscillation amplitude, was equal to ~1 V, and the images were acquired at 2 Hz scan frequency in 2 × 2 μm^2 scan areas. The grazing incidence X-ray scattering (GIXS) images were taken at the Cornell High Energy Synchrotron Source (CHESS) D1 station. A wide bandpass (1.47%) double-bounce multilayer monochromator supplied an intense beam of 10.1 keV photons. These were impinged onto the sample surface at various incident angles ranging from below the critical angle of the film and above the critical angle of the substrate. The sample was mounted on a sample goniometer to control the incident angle and the sample azimuth. An accurate calibration of the incident angle was performed in situ by measuring the X-ray reflectivity from the sample using an ion chamber. Scattering intensities were recorded with an area detector (Medoptics) with a resolution of 47.19 μm per pixel and a total area of about 50 mm by 50 mm at a distance of 92~98 mm from the sample. The intense scattering in the incident plane was blocked with a 1.5 mm wide tantalum rod. Exposure times under these conditions ranged from 1 to 30 s depending on contrast and sample quality.

Fabrication and Characterization of OFET Devices. Organic field-effect transistors were fabricated in the bottom gate, bottom contact configuration on heavily doped n-type Si substrates as the gate and a thermally grown 250 nm silicon dioxide as the dielectric layer (Silicon Quest). The source and drain electrodes were patterned using standard photolithography methods and were deposited on the SiO_2 by sputter deposition of ~5 nm of titanium and 50 nm of gold. The channel lengths were 5, 10, and 25 μm, and the ratio of channel width to channel length was W/L = 50. The devices were plasma etched (IPC Plasma etcher, 250 W, 15 min, temperature reached 168 °C) and were stored in a desiccator until ready for polymer deposition. Prior to polymer deposition, device surfaces were treated with UV/ozone irradiation at 120 °C for 10 min and subsequently with octyltrichlorosilane (OTS-8, Acros) by immersing the devices in a ~40 mM solution in hexadecane at room temperature for 2 h. The treatment with OTS-8 was performed in a glovebox under nitrogen. The devices were then rinsed in air with dry toluene and were dried with nitrogen flow followed by vacuum for at least one hour. The polymer films were deposited in air by drop casting 5 μL of a 0.75 mg/mL solution in dry chloroform and were allowed to dry in a glass Petri dish saturated with chloroform. The polymer solutions were filtered through 0.2 μm PTFE filters prior to film deposition. The devices were then further dried under vacuum overnight and then were annealed at 150 °C on a hot plate in a glovebox. The devices were briefly exposed to air while being set on the probe station. The OFET devices of the polymers were characterized using Agilent 4155C Semiconductor Parameter Analyzer and Micromanipulator S6 Probe Station in air. When measuring current−voltage curves and transfer curves, V_G was scanned from −80 V to +40 V. The mobility was evaluated from the saturation regime at $V_G = -80$ V using the slope of the line drawn through the linear part of an $I_{SD}^{1/2}$ versus V_G plot (−80 to −60 V), where V_G and I_{SD} are the gate voltage and drain-source current, respectively.

Table 1. Chemical, Optical, and Electrochemical Properties of the Polymers

polymer	M_n	M_w	PDI	DP_n[a]	λ_{max} (nm)[b]	Eg (eV)[c]	IP (eV)[d]
PTzQT-6	4100	6000	1.5	5.1	574, 622	1.8	5.0
PTzQT-12	7200	17 100	2.4	6.3	579, 629	1.8	5.1
PTzQT-14	8700	15 800	1.8	7.0	582, 629	1.8	5.1

[a] Calculated from the number-averaged molecular weight (M_n). [b] Absorption maxima of the polymer thin films spin coated on glass slides from chloroform solutions. [c] Evaluated from the onset of the absorption spectra of the polymer thin films. [d] Evaluated from the onset of the oxidation potentials in cyclic voltammetry.

Results and Discussions

Polymer Properties. The molecular weight of the polymers, which was evaluated by GPC using the polystyrene standard, M_n = 4100−8700, M_W = 6000−17100, is listed in Table 1. The degree of polymerization (DP_n) was calculated with M_n to be 5−7 indicating that the polymer main chain consists of 30−42 rings including alkylthiophenes and thiazolothiazoles.

The normalized absorption spectra of the polymers in the solid state (Figure 1) provided a shoulder at 500~550 nm and two absorption maxima (λ_{max}) at 570~580 and 620~630 nm, respectively; λ_{max} values are listed in Table 1. Interestingly, the shoulder in the shorter wavelength region has red-shifted and the absorbance of the peak in the longer wavelength region has increased as the side chain elongated. This implies that the polymer with longer alkyl chain forms relatively higher order structure in the thin film. The band gap (Eg) of the polymers, evaluated from the onset of the absorption spectra of the polymer films, was 1.8 eV (Table 1), which was found to be 0.2 eV smaller than that of rrP3HT (2.0 eV).

The IP of the polymers, calculated from the onset of the oxidation potentials obtained from the cyclic voltammetry (CV) of the polymer films, was 5.0−5.1 eV. **PTzQT-6** exhibited a slightly smaller value than the other PTzQTs. These values were about 0.1−0.2 eV larger than that of rrP3HT (4.9 eV) measured under the same conditions ensuring higher oxidative stability.

(15) Li, Y; Ding, J.; Day, M.; Tao, Y.; Lu, J.; D'iorio, M. *Chem. Mater.* **2004**, *16*, 2165.

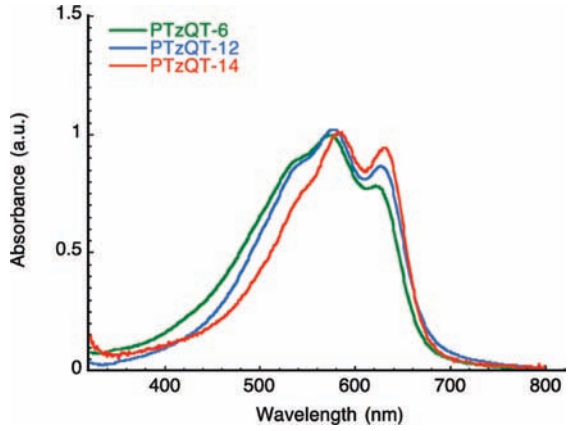

Figure 1. UV−vis absorption spectra of the polymer thin films.

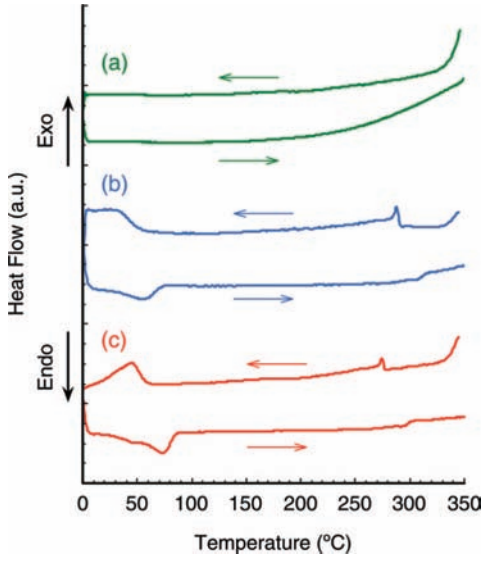

Figure 2. DSC thermograms of (a) **PTzQT-6**, (b) **PTzQT-12**, and (c) **PTzQT-14**. The leftward arrows and the rightward arrows represent the heating and the cooling processes, respectively.

Table 2. Transition Temperatures of the Polymers[a]

	heating (°C)		cooling (°C)	
polymer	T_1	T_2	T_1	T_2
PTzQT-6				
PTzQT-12	55	303	30	287
PTzQT-14	70	288	49	274

[a] T_1 and T_2 correspond to the lower and higher transition temperatures, respectively, appearing on the DSC thermograms.

This greater stability can also be attributed to the introduction of the electron-deficient thiazolothiazole ring in the polymer backbone.

Thermal analysis of the polymers was carried out by differential scanning calorimetry (DSC). The DSC thermograms of the polymers are depicted in Figure 2; transition temperatures are listed in Table 2. **PTzQT-12**, **-14** provided two endothermic peaks in the heating process and two exothermic peaks in the cooling process indicating the existence of a mesophase. The peaks at lower (T_1) and higher (T_2) temperatures could be assigned to side chain melting and backbone melting, respectively. Meanwhile, **PTzQT-6**, which possesses shorter alkyl chains, exhibited no endothermic or exothermic peaks in the range of 0−350 °C suggesting no evidence of mesophase. **PTzQT-14** exhibited a narrower mesophase temperature range relative to **PTzQT-12** by increasing T_1 and decreasing T_2. The fact that the longer side chain polymer gives higher T_1 and lower T_2 can be explained as follows. Longer side chains attached to the polymer backbone may be more likely to interact with each other, and therefore a higher temperature (T_1) should be required to cause their melting; once they are melted, they should act like a good solvent and lead to a lowering of the melting temperature of the backbone (T_2). It thus seems that the alkyl side chain behaves as if it is an independent alkane group. Interestingly, this thermal behavior in PTzQTs is quite opposite from that in PBTTTs.[7b] In PBTTTs, T_1 decreases as the side chain elongates probably because of the increased flexibility of the polymer chain in the longer side chain polymer. The thermal behavior of the side chain and the backbone may be dependent in PBTTTs. This difference in the thermal behavior between PTzQTs and PBTTTs is thus, apparently, in good agreement with that PTzQTs show relatively lower T_1 (<50 °C) than PBTTT (>100 °C).

Microstructural Study of the Polymer Thin Films. The microstructure of the polymer thin films was studied using grazing incidence X-ray scattering (GIXS). For the GIXS measurements, the polymer thin films were prepared by drop casting the chloroform solution of the polymers on OTS-8 treated silicon wafers with native oxide layer, and the films were annealed at 150 °C for 30 min. Figure 3 displays the two-dimensional GIXS images of the polymer thin films, and Figure 4 shows the GIXS patterns plotted along the $\mathbf{q}_z$ and $\mathbf{q}_{||}$ axes, respectively, from the two-dimensional images. In all polymers, peaks corresponding to the lamellar *d*-spacing only appear along the $\mathbf{q}_z$ axis (out-of-plane). This indicates edge-on orientation of the polymer lamellae on the SiO_2 surface as is common for rrP3HT.[1d] In the lamellae, conjugated planes must be roughly vertical to the surface plane, forming a face-to-face $\pi-\pi$ stacking. However, the conjugated planes are apparently somewhat tilted with a variety of degrees.[16,17] The lamellar *d*-spacings are evaluated to be 14.4, 20.7, and 22.1 Å for **PTzQT-6**, **-12**, and **-14**, respectively. These values indicate that vertically adjacent polymer backbones are packed very closely, that is, the *d*-spacing for rrP3DDT (DD = dodecyl) is ∼25 Å. The lamellar ordering feature for PTzQTs is significantly affected by the side chain length. **PTzQT-6** exhibited three orders for the lamellar peaks, whereas the longer side chain polymers, **PTzQT-12** and **-14**, provided four and five orders, respectively, indicating more highly ordered lamellar structure in the longer side chain polymers (Figure 4a). A plausible explanation for this trend is that longer alkyl chains are more likely to interlock with adjacent polymer chains giving highly ordered structures.

The peaks in the $\mathbf{q}_{||}$ axis appeared to be somewhat broad (Figure 4b). The peaks in the smaller angle region, $\mathbf{q}_{||} = 1.4-1.5$ Å^{-1}, can be assigned to the scattering from the alkyl side chains (4.1−4.3 Å), and the peaks in the wider angle region, $\mathbf{q}_{||} = 1.7-1.8$ Å^{-1}, correspond to $\pi-\pi$ stacking distance (3.5−3.7 Å). In PBTTTs, the peak at around $\mathbf{q}_{||} = 1.4$ Å^{-1} is reported to correlate with the length of the repeating unit of the polymer (∼13 Å). In PTzQTs, however, the estimated length of the repeating unit is ∼20 Å and does not correlate with the peak at $\mathbf{q}_{||} = 1.4-1.5$ Å^{-1}. This peak has intensified in the longer side

(16) DeLongchamp, D. M.; Kline, R. J.; Lin, E. K.; Fischer, D. A.; Richter, L. J.; Lucas, L. A.; Heeney, M.; McCulloch, I.; Northrup, J. E. *Adv. Mater.* **2007**, *19*, 833.
(17) Chabinyc, M. L.; Toney, M. F.; Kline, R. J.; McCulloch, I.; Heeney, M. *J. Am. Chem. Soc.* **2007**, *129*, 3226.

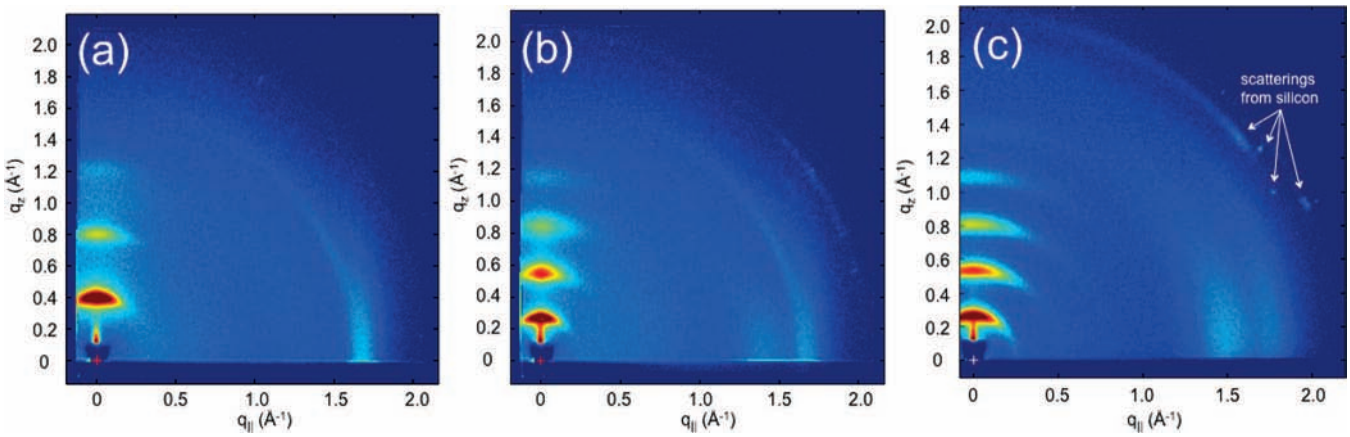

Figure 3. Two-dimensional GIXS image of (a) **PTzQT-6**, (b) **PTzQT-12**, and (c) **PTzQT-14** (after annealing).

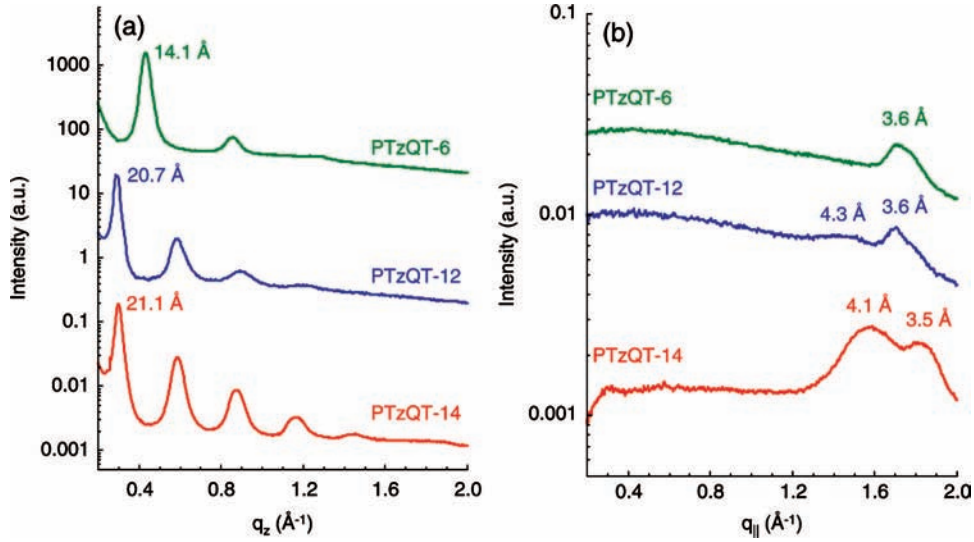

Figure 4. GIXS patterns of the polymer thin film cast on OTS-8 treated SiO_2 surfaces (a) out-of-plane and (b) in-plane patterns of **PTzQT-6**, **-12**, and **-14** (after annealing).

chain polymers. This trend may be supportive for that we assigned the peak as the scattering from the alkyl side chains since the longer alkyl chains have more electrons to scatter and thus should give stronger peak. These scattering characteristics in wide-angle region, in which PTzQTs show only one peak corresponding to the backbone ordering, suggest the lower $\pi-\pi$ stacking crystallinity of PTzQTs as compared to PBTTTs that show two peaks for the backbone ordering.

In PBTTTs or PQT, experimental data showed that the alkyl side chains tilt around 50° relative to the normal of the unit cell basal plane and that the polymers form a high degree of side chain interdigitation (Figure 5a).[13] In PTzQTs, however, side chains are not tilted in the same manner. If the side chains are tilted in PTzQTs, the alternating side chains should bump into each other and hence cause a significant sterical-driven twist of the conjugated backbone. The absorption spectra do not support a large destruction of π-conjugation. One might then expect that the side chains can head straightforward roughly along the normal of the unit cell basal plane and form side chain interdigitation or side chain crystallization. However, unequally distributed side chains, where the distances between the carbon atoms at the 3 position of the thiophene rings are approximately 10 Å and 12 Å, do not allow uniform and high degree of interdigitation in this system. In addition, relatively lower

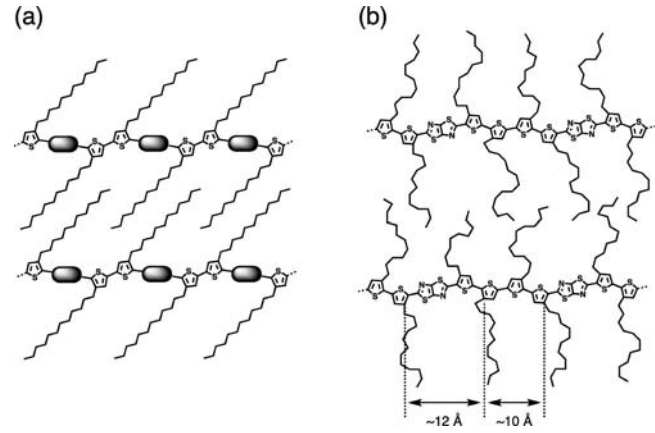

Figure 5. Schematic illustrations for (a) the packing structure of PQT and PBTTT with dodecyl side chain with uniform side chain interdigitation and (b) proposed packing structure of **PTzQT-12** with disordered side chains.

π-stacking crystallinity in this system compared with PBTTT should be indicative of loss of side chain interdigitation. We thereby propose that in this system the side chains form only a small degree of side chain interdigitation that can slightly interlock adjacent polymers and that are disordered to fill out the free volume between the neighboring side chains. This

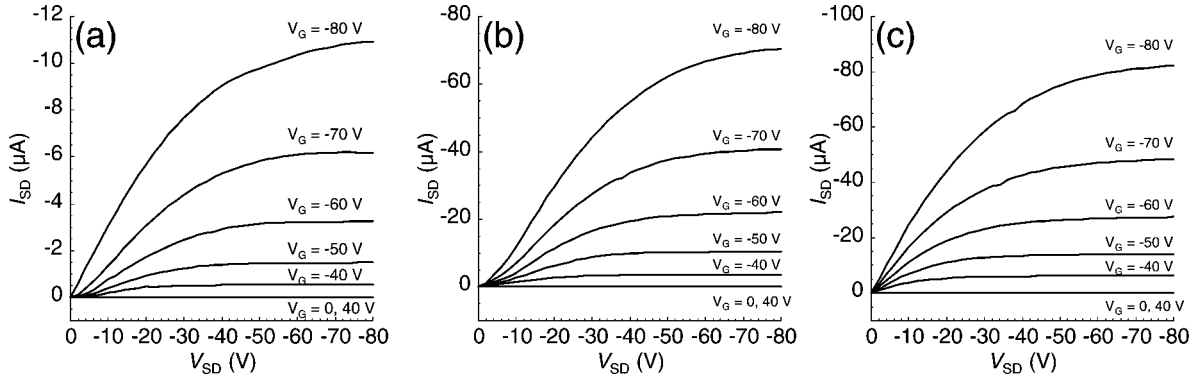

Figure 6. Output curves of the annealed polymer devices for $L = 25$ μm, $W = 1250$ μm at different V_G: (a) **PTzQT-6**, (b) **PTzQT-12**, and (c) **PTzQT-14**. I_{SD}, V_{SD}, and V_G represent source-drain current, source-drain voltage, and gate voltage, respectively.

disordered model is in agreement with the thermal behavior of the polymer that the side chains act like an independent alkane group. Although the side chains are likely to be disordered, the polymer lamellae are still closely packed and highly ordered promoting a three-dimensional packing order in the thin film. This is probably due to the high coplanarity and rigidity of the thiazolothiazole−thiophene backbones, which also promotes a strong π connectivity throughout the structure.

OFET Properties. OFET properties of the polymers were evaluated using bottom contact devices fabricated by drop casting the room temperature chloroform solution of the polymers on the SiO_2 gate dielectric treated by octytrichlorosilane (OTS-8). The devices were annealed for 30 min at 150 °C, which is in the mesophase temperature range of the polymers (∼50 to ∼290 °C), in a glovebox under nitrogen prior to measurement. Thermal annealing has been shown to improve device performance ∼2-fold for mobility and 2∼3 orders of magnitude for on/off ratio in this system[14] as typical for polymers exhibiting mesophase.[4,5a,6a,7,8] It is interesting that **PTzQT-6**, which exhibits no mesophase, also showed an increase in both mobility and on/off ratio after annealing.[9] Although the thiazolothiazole moiety is a potential building block for n-type semiconductors,[18] PTzQTs did not show electron mobility. Further investigation is necessary to realize n-type behavior in thiazolothiazole containing soluble polymers.

Figures 6 and 7 provide the typical current−voltage characteristics of annealed polymer devices with $L = 25$ μm, where I_{SD}, V_{SD}, and V_G represent source-drain current, source-drain voltage, and gate voltage, respectively. The output curves (Figure 6) show good saturation and some nonlinear behavior in the range of lower V_{SD}. This nonlinear behavior may originate from contact resistance or trap sites. The threshold voltage (V_T) derived from the onset of the transfer curve (Figure 7) was negatively shifted to ∼ −30 V (Table 3) also suggesting the existence of some trap sites. The mobility (μ) of the polymer devices was calculated in the saturation regime using the slope derived from $(-I_{SD})^{1/2}$ versus V_G plots between −80 to −60 V (Figure 7).[19] Table 3 shows the summarized μ values for the annealed devices with channel length (L) of 25, 10, and 5 μm. All polymer devices showed very good reproducibility. **PTzQT-12** and **-14** afforded very high mobility of, for example, 0.050−0.11 and 0.12−0.17 cm^2/Vs, respectively, for $L = 25$ μm. The highest mobility was obtained from a **PTzQT-14**

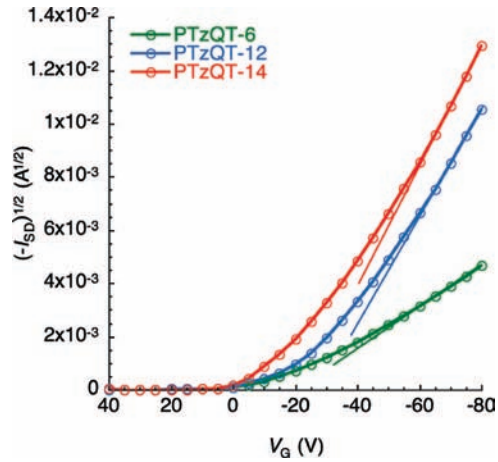

Figure 7. Transfer characteristics of the annealed polymer devices for $L = 25$ μm, $W = 1250$ μm at $V_{SD} = -80$ V.

device with $L = 5$ μm to be 0.30 cm^2/Vs. These values are surprisingly high for low molecular weight semiconducting polymers.[20,21] This is certainly the necessary consequence of the highly ordered three-dimensional structure of the polymer lamellae as revealed by GIXS.

Interestingly, as seen in Table 3, PTzQTs with longer alkyl chain showed higher mobility. **PTzQT-14** tended to exhibit higher mobility relative to **PTzQT-12**, and **PTzQT-6**, on the other hand, showed 1 order magnitude lower values than these two. The transfer characteristics of the polymers as shown in Figure 4 also indicate this tendency. The fact that mobility is influenced by alkyl chain length is consistent with the GIXS study that the longer alkyl chain polymer tends to show higher lamellar ordering. This trend is further supported by the

(18) (a) Ando, S.; Nishida, J.; Tada, H.; Inoue, Y.; Tokito, S.; Yamashita, Y. *J. Am. Chem. Soc.* **2005**, *127*, 5336. (b) Mamada, M.; Nishida, J.; Kumaki, D.; Tokito, S. *Chem. Mater.* **2007**, *19*, 5404.

(19) Mobilities of the polymers vary dependent on the range of V_G used when deriving the slope from $(-I_{SD})^{1/2}$ vs V_G plots. For example, the mobility, 0.17, for the **PTzQT-14** device with $L = 25$ μm increases to 0.18 when the slope is derived from the V_G range between−80 to−70 V and slightly decreases to 0.15 and 0.14 when the slope is derived from the range between−80 to−50 V and−80 to−40 V, respectively.

(20) Zhang, R.; Li, B.; Iovu, M. C.; Jeffries-EL, M.; Sauvé, G.; Cooper, J.; Jia, S.; Tristram-Nagle, S.; Smilgies, D. M.; Lambeth, D. N.; McCullough, R. D.; Kowalewski, T. *J. Am. Chem. Soc.* **2006**, *128*, 3480.

(21) (a) Kline, R. J.; McGehee, M. D.; Kadnikova, E. N.; Liu, J.; Fréchet, J. M. J. *Adv. Mater.* **2003**, *15*, 1519. (b) Kline, R. J.; McGehee, M. D.; Kadnikova, E. N.; Liu, J.; Fréchet, J. M. J.; Toney, M. F. *Macromolecules* **2005**, *38*, 3312. (c) Zen, A.; Pflaum, J.; Hirschmann, S.; Zhuang, W.; Jaiser, F.; Asawapirom, U.; Rabe, J. P.; Scherf, U.; Neher, D. *Adv. Funct. Mater.* **2004**, *14*, 757.

Table 3. Mobility, On/Off Ratio, and Threshold Voltage (V_T) of the Polymer Devices.

	mobility (cm^2/Vs)[a]				
polymer	$L = 25\ \mu m$	$L = 10\ \mu m$	$L = 5\ \mu m$	on/off ratio[b]	V_T (V)[c]
PTzQT-6	0.013−0.020	0.020−0.031	0.033−0.050	10^5−10^7	−17 to −27
PTzQT-12	0.050−0.11	0.11−0.14	0.11−0.23	10^5−10^7	−22 to −31
PTzQT-14	0.12−0.17	0.15−0.21	0.20−0.30	10^5−10^7	−23 to −30

[a] Evaluated from the saturation regime ($V_G = -80 \sim -60$ V) at $V_{SD} = -80$ V. [b] Calculated from $I_{SD} = -80$ V (on) and 40 V (off). [c] Evaluated from the onset of the transfer curves.

morphological studies of the polymer thin films and will be discussed later in this paper. In addition, to our knowledge, the effect of the alkyl chain length in the PTzQT system contrasts with the regioregular poly(3-alkylthiophene) (rrP3AT) system. rrP3DDT (DD = dodecyl) shows only similar mobility compared to rrP3HT in our work[22] and according to other reports may show even much lower mobility.[23]

The devices with shorter channel length tended to exhibit higher mobility. One hypothesis for this tendency is that in the shorter channel length there should be fewer domain boundaries, and this tends to decrease the chance that the carrier will be trapped at the boundary. The other possibility is short channel effects, which have been described and observed in OFETs for channel length < 10 μm.[24] The output curves did not show as good saturation behavior as those for $L = 25\ \mu$m (see Supporting Information) suggesting that short channel effects may be included.

In addition, we have examined the effect of annealing temperature on mobility. Five different **PTzQT-12** devices were fabricated at the same time using the same polymer solution and were annealed at 100, 150, 200, 250, and 300 °C. The mobility of the devices for $L = 5\ \mu$m annealed at 100, 150, and 200 °C was 0.17−0.20 cm^2/Vs, while those annealed at 250 and 300 °C showed slightly lower values, 0.13−0.14 cm^2/Vs, suggesting that annealing at too high a temperature may degrade FET performance. Although the AFM study did not show any morphological difference, some structural change might have occurred.

The current on/off ratio of the polymer devices at −80 V/40 V were as high as 10^7 (Table 3). These high on/off ratios can be attributed to the large IP of the polymers preventing the oxygen doping that increases the off current. However, the on/off ratio varied in the range of 3 orders of magnitude (10^5−10^7), and perhaps this variation depends on device quality. Conditions such as temperature and humidity at the time of device fabrication might affect the device quality.

Devices with these polymers maintained good performance even after the devices were stored in air in the dark for 30 days (at r.t., 45∼65% humidity). The mobilities and the on/off ratios of the polymer devices with $L = 10\ \mu$m before and after standing in air for the period are summarized in Table 4. The devices showed only a slight decrease in mobility under this condition. The changes in on/off ratio seem to be more interesting. As seen in Figure 8, the on/off ratio for the device with **PTzQT-6** drastically decreased from 1×10^5 to 70; however, the **PTzQT-12** device decreased from 5×10^5 to 4×10^3, and the **PTzQT-14** device slightly decreased from 1×10^6 only to 5×10^5. This result suggests that longer alkyl chains drive lamellar order which helps to possibly protect the polymer backbone away from ambient air and to protect them from humidity and oxygen (which may degrade device performances) leading to higher stability.

Table 4. Mobility and On/Off Ratio of the Polymer Devices Stored in Air in the Dark

	mobility (cm^2/Vs)[a,b]		on/off ratio[a,c]	
polymer	initial[d]	30 days[e]	initial[d]	30 days[e]
PTzQT-6	0.020	0.011	1×10^5	70
PTzQT-12	0.11	0.085	5×10^5	4×10^3
PTzQT-14	0.18	0.15	1×10^6	5×10^5

[a] For the devices with $L = 10\ \mu$m. [b] Evaluated from the saturation regime ($V_G = -80 \sim -60$ V) at $V_{SD} = -80$ V. [c] Calculated from $I_{SD} = -80$ V (on) and 40 V (off). [d] Initial, measured immediately after the devices were fabricated. [e] Thirty days, measured 30 days after the devices were stored in air, in the dark at r.t. and 45∼65% humidity.

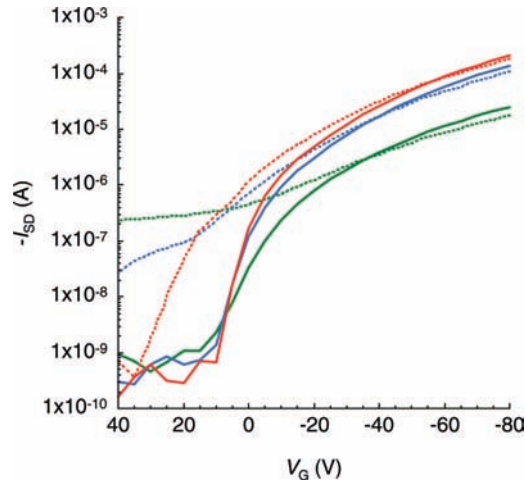

Figure 8. Variation in transfer characteristic of devices with **PTzQT-6** (green line), **PTzQT-12** (blue line), and **PTzQT-14** (red line) for $L = 10\ \mu$m and $W = 500\ \mu$m after being stored for 30 days in air, in the dark. Solid lines, initial; dotted lines, after 30 days.

Morphological Study of the Polymer Thin Films. The morphology of the polymer thin films on the transistor surface (annealed at 150 °C) was studied using tapping mode atomic force microscopy (AFM). Figure 9 shows AFM images of the polymer thin films inside the channel of transistors after annealing, where the upper row (Figure 9a−c) shows topographic images and the lower row (Figure 9d−f) shows phase contrast images. In all cases, well-defined nanograins are the dominant surface morphological features. These morphologies that display small domains are in sharp contrast to those of rrP3HT, which affords nanofibrillar morphology,[20,21,25] or PQT and PBTTT, which affords very large crystalline domains with

(22) Sauvé, G.; Javier, A.; Liu, J.; Zhang, R.; Kowalewski, T.; McCullough, R. D. Manuscript in preparation, 2009.
(23) (a) Kaneto, K.; Lim, W. Y.; Takashima, W.; Endo, T.; Rikukawa, M. *Jpn. J. Appl. Phys.* **2000**, *39*, L872. (b) Babel, A.; Jenekhe, S. A. *Synth. Met.* **2005**, *148*, 169. (c) Park, Y. D.; Kim, D. H.; Jang, Y.; Cho, J. H.; Hwang, M.; Lee, H. S.; Lim, J. A.; Cho, K. *Org. Electron.* **2006**, *7*, 514.
(24) (a) Chabinyc, M. L.; Lu, J.-P.; Street, R. A.; Wu, Y.; Liu, P.; Ong, B. S. *J. Appl. Phys.* **2004**, *96*, 2063–2070. (b) Haddock, J. N.; Zhang, X.; Zheng, S.; Zhang, Q.; Marder, S. R.; Kippelen, B. *Org. Electron.* **2006**, *7*, 45.

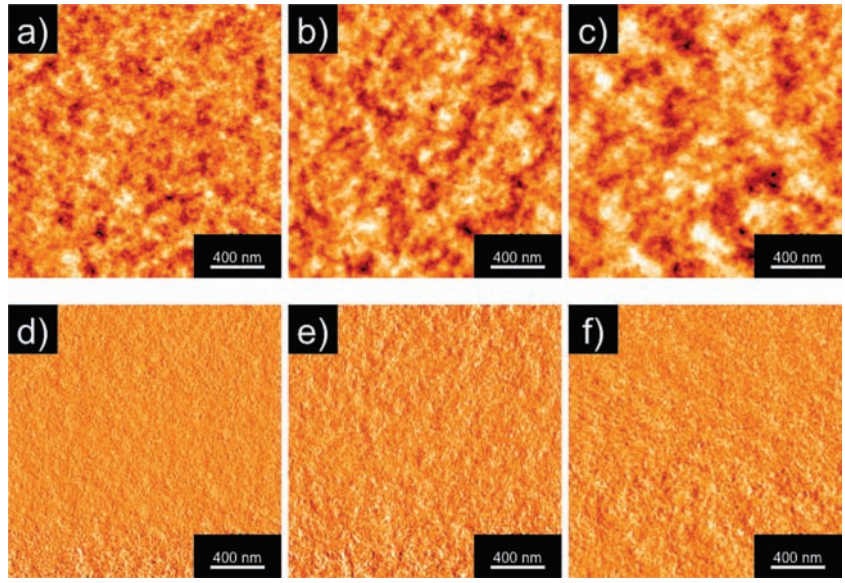

Figure 9. Tapping mode AFM images of (a, d) **PTzQT-6**, (b, e) **PTzQT-12**, and (c, f) **PTzQT-14** on the OFET devices after annealing at 150 °C for 30 min. The upper row (a−c) shows topographic images, and the lower row (d−f) shows phase contrast images.

extended smooth, terracelike structures evidently rooted in their lamellar morphology. This is probably due to their low molecular weight and perhaps disordered side chains. Previous study in rrP3HT has revealed that the width of nanofibrils increased linearly with the molecular weight.[20] The nanofibrils have large domains but give rise to large domain boundaries (disordered regions). Those disordered regions are believed to cause a disconnection of $\pi-\pi$ electron system and thereby limit the carrier transport between the neighboring domains. However, the small domains in these PTzQT morphologies seem to be well connected with each other, diluting the disordered regions, and are packed into isotropic amorphous-like superstructures. This developed interdomain connectivity should encourage the interdomain carrier transport and allow high mobility in PTzQTs despite the low molecular weight. Sirringhaus has suggested that disordered and amorphous systems with good domain connectivity could lead to high mobility[2d] as exemplified by PTzQT system, dithienopyrrole−thiophene system,[11] and in work by Zhang et al.[9]

Closer examination of the topological images of PTzQT thin films indicates that the nanograins appearing on the surface are tightly aggregated resulting in somewhat larger grains with different lateral correlation length. The lateral correlation length of the nanograins seems to be dependent on the side chain of the polymers. Figure 10a shows typical cross section profiles of topographic images for PTzQT thin films. These profiles suggest that PTzQT with a longer side chain tends to give longer lateral correlation length of the nanograins. To further quantify these profiles, spatial Fourier transform of the topographic images in polar coordinates was performed to obtain the power spectral density (PSD), P (**q**), versus wavevector **q** (Figure 10b).[26] The PSD describes the contribution of different spacial frequencies to the surface plane of the thin films, for example, the frequency of lateral variation over a range of length scales.

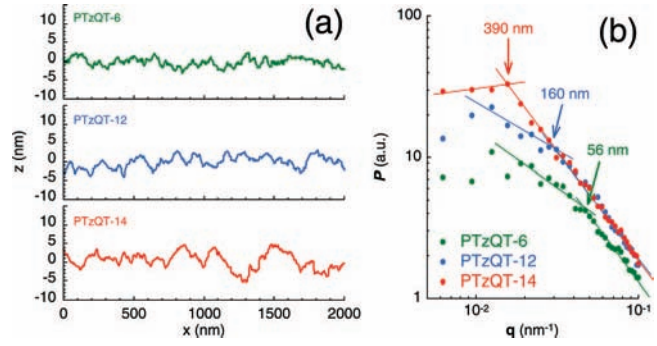

Figure 10. (a) Typical cross section profiles of AFM topographic images for PTzQT thin films and (b) power spectral density (PSD) P versus wavevector **q** calculated from the spatial Fourier transform of the topographic images in polar coordinates.

It is apparent that all surfaces of PTzQT thin films reveal two different regimes (two different curve slopes), that is, two different power law dependences of PSD. Cross over of these two regimes occur at $\mathbf{q} = 0.11$, 0.038, and 0.016 nm^{-1} for **PTzQT-6**, **-12**, and **-14**, and these **q** values correspond to the lateral correlation length of 56, 160, and 390 nm, respectively, indicating that PTzQTs with a longer side chain have longer lateral correlation length. This result implies that PTzQTs with a longer side chain possess superior carrier transport pathway in the film surface. This trend in morphology is positively correlated to the trend in mobility.

PTzQTs have a rather short polymer chain and some disordering in side chain packing, which may be preventing the formation of a well-defined terrace that gives very high carrier movement.[13] However, PTzQT with a longer side chain (**PTzQT-14**) exhibits grains with lateral correlation length of submicrometer size in the film surface, and this still seems to give efficient enough carrier movement, which has been proven by the OFET characterization.

Conclusions

We have presented the microstructural and morphological studies on a series of thiazolothiazole−thiophene copolymers

(25) Yang, H.; Shin, T. J.; Yang, L.; Cho, K.; Ryu, C. Y.; Bao, Z. *Adv. Funct. Mater.* **2005**, *15*, 671.
(26) (a) Chua, L.-L.; Ho, P. K. H.; Sirringhaus, H.; Friend, R. H. *Adv. Mater.* **2004**, *16*, 1069. (b) Jung, Y.; Kline, R. J.; Fischer, D. A.; Lin, E. K.; Heeney, M.; McCulloch, I.; DeLongchamp, D. M. *Adv. Funct. Mater.* **2008**, *18*, 742.

(PTzQTs). It has been proposed in literature that highly regular side chain interdigitation may be a key factor in facilitating formation of highly regular lamellar structures and facilitating high carrier mobility in field-effect transistors. Interestingly, despite the lack of side chain interdigitation and ordering, which may be understood as a consequence of uneven side chain placement along the backbone preventing their regular packing, our polymers exhibited a very high degree of lamellar ordering and high carrier mobilities. At the same time, their surface morphology turned out to be very different from the surface morphology of PBTTT. Whereas the latter were shown to form extended smooth, terracelike structures associated with the side chain interdigitation, the surfaces of our systems had the character of disordered fractals composed of ill-defined "granular" domains. More detailed quantitative Fourier analysis of this morphology revealed the presence of lateral correlations with the correlation length increasing with the length of the alkyl side chains. The observed height correlation length may be viewed as the parameter describing the fluctuations of the lamellar order from "perfect" planarity. Our results strongly suggest that the lateral correlation length of disordered surfaces is a key structural parameter for transport with longer correlations favoring higher carrier mobility.

Altogether, these results indicate that a high degree of interdigitation and resulting flat terracelike structures like those observed for PBTTT are not the sole necessary condition for high carrier mobility. Evidently, equally high mobilities may be achieved in noninterdigitating systems, where domains, in which the polymer lamellae are highly ordered, are packed into isotropic amorphous-like superstructures. We believe that this is an important and new finding significantly broadening our understanding of structure−transport relationships in semiconducting polymers.

Acknowledgment. Financial support was provided by the National Science Foundation (CHE0415369) and the Air Force Office of Scientific Research (FA9550-07-1-0245). A portion of this work was carried out at the Cornell High Energy Synchrotron Source, Cornell University, and is supported by the National Science Foundation (DMR-0225180).

Supporting Information Available: Cyclic voltammograms of the polymers, transistor characteristics of the polymer devices. This material is available free of charge via the Internet at http://pubs.acs.org.

JA801475H